Medical Engineering and Physics 126 (2024) 104143

Contents lists available at ScienceDirect

Medical Engineering and Physics

journal homepage: www.elsevier.com/locate/medengphy

Paper

Critical loss of primary implant stability in osteosynthesis locking screws under cyclic overloading

Juan D. Silva-Henao [a,b,*], Sophie Schober [c], Dieter H. Pahr [a,b], Andreas G. Reisinger [a,b]

[a] Karl Landsteiner University of Health Sciences, Department of Anatomy and Biomechanics, Division Biomechanics, Dr. Karl-Dorrek-strae 30, 3500, Krems, Austria
[b] Institute of Lightweight Design and Structural Biomechanics, Technische Universität Wien, Vienna, Austria
[c] Institute of Science and Technology Austria (ISTA), Am Campus 1, 3400 Klosterneuburg, Austria

ARTICLE INFO

Keywords:
Osteosynthesis screw
Primary implant stability
Damage
Failure load
Anatomical loading

ABSTRACT

Primary implant stability, which refers to the stability of the implant during the initial healing period is a crucial factor in determining the long-term success of the implant and lays the foundation for secondary implant stability achieved through osseointegration. Factors affecting primary stability include implant design, surgical technique, and patient-specific factors like bone quality and morphology. In vivo, the cyclic nature of anatomical loading puts osteosynthesis locking screws under dynamic loads, which can lead to the formation of micro cracks and defects that slowly degrade the mechanical connection between the bone and screw, thus compromising the initial stability and secondary stability of the implant. Monotonic quasi-static loading used for testing the holding capacity of implanted screws is not well suited to capture this behavior since it cannot capture the progressive deterioration of peri-implant bone at small displacements. In order to address this issue, this study aims to determine a critical point of loss of primary implant stability in osteosynthesis locking screws under cyclic overloading by investigating the evolution of damage, dissipated energy, and permanent deformation. A custom-made test setup was used to test implanted 2.5 mm locking screws under cyclic overloading test. For each loading cycle, maximum forces and displacement were recorded as well as initial and final cycle displacements and used to calculate damage and energy dissipation evolution. The results of this study demonstrate that for axial, shear, and mixed loading significant damage and energy dissipation can be observed at approximately 20 % of the failure force. Additionally, at this load level, permanent deformations on the screw-bone interface were found to be in the range of 50 to 150 mm which promotes osseointegration and secondary implant stability. This research can assist surgeons in making informed preoperative decisions by providing a better understanding of the critical point of loss of primary implant stability, thus improving the long-term success of the implant and overall patient satisfaction.

1. Introduction

Osteosynthesis screws, are widely used in orthopedic surgery to stabilize and join bone fracture fragments (Fig. 1). They play a crucial role in the healing process by serving as the primary connection element between an implant, such as a plate, and the broken bone fragments. To ensure a successful outcome, it is vital to maintain a secure connection between the implanted screw and the bone, referred to as implant stability. Implant stability is generally divided into two stages: primary implant stability, occurring immediately after screw implantation, and secondary implant stability, which occurs after osseointegration takes place [1]. The transition from primary to secondary implant stability is accomplished by stimulating mechanoreceptors in the peri-implant bone tissue through progressive loading and unloading of the implant thus promoting the bone remodeling process [2]. Research has shown that implant movement between 50 and 150 micrometers promotes osseointegration and secondary implant stability [3,4]. However, excessive movement at the implant-bone interface due to overloading can result in complications such as fibrous encapsulation [4] damage or breakage of peri-implant trabecular bone [5], and even failure of osseointegrated implants [6]. These complications often lead to screw loosening, requiring costly and uncomfortable revision surgeries that strain the healthcare system and negatively impact the patient's recovery process and quality of life.

* Corresponding author.
E-mail address: juan.silva@kl.ac.a (J.D. Silva-Henao).

https://doi.org/10.1016/j.medengphy.2024.104143
Received 12 April 2023; Received in revised form 26 February 2024; Accepted 3 March 2024
Available online 4 March 2024

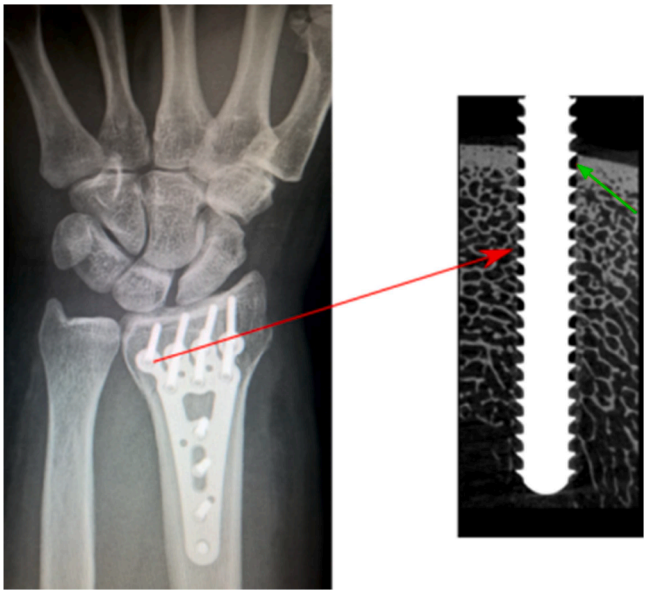

Fig. 1. X-ray image of a distal radius fracture treated with osteosynthesis plate. Close up image shows poor contact between the implanted screw and bone marked by a green arrow.

Several efforts have been made to improve implant success by quantifying and predicting the holding capacity and stability of implanted osteosynthesis screws through mechanical testing which can lead to better implantation strategies in surgical planning, resulting in better patient outcomes [1]. Studies have shown that the mechanical performance of osteosynthesis screws is closely related to the peri-implant bone architecture parameters, such as bone volume fraction (BV/TV) [7], trabecular thickness (Tb.Th.) [8], bone mineral density (BMD) [9], cortical thickness (Ct.Th.) [10] and peri-implant bone volume [11]. Additionally, pre-, and post-implantation measurements, such as drilling force and insertion torque, have been shown to be reliable indicators of screw failure force and construct stiffness [12]. This is particularly relevant as CT-derived morphometric values such as BV/TV can be used as a tool for implantation site planning thus optimizing the screw holding capacity and stability and in turn increasing the chances of implant success. Furthermore, different failure configurations have been tested including pull-out loading [11,13], shear loading [10,13], push-in loading or screw perforation [14]. Since most implanted screws are subjected to a combination of axial bending and shear forces [15,16], it is important to understand the mechanical performance of the screws under these various loading configurations and how the underlying bone architecture affects it in order to optimize the screw design and improve implant success. To sum up, osteosynthesis screws failure is due to a combination of several factors including implantation site morphology, damage caused by the surgeon while implanting the screw, loading environment, and the correct definition of the failure point is key to producing better preoperative tools that can be provided to a surgeon, ultimately improving the overall patient recovery time and satisfaction.

It is common practice to quantify the screw holding capacity by means of monotonic loading until a maximum bearable load is reached. The failure point of the implanted screw is taken as the maximum load reached under specific loading configurations, such as pull-out, cut-through, and push-in [11,13,17,18]. The initial stability of the implant construct is represented by either the slope of linear portion of the force-displacement curve [19] or measured using other techniques such as resonance frequency analysis [20–22]. However, it's important to note that these methods have their limitations. Monotonically loading a screw until failure does not accurately reflect the dynamic nature of physiological loading and it has been shown that maximum load, for example, pull-out force, is not a suitable predictor for other failure modes such as screw loosening [23,24] or migration [25]. Furthermore, under cyclic loading the increasing displacements in the bone-screw interface propagate micro-crack and exploit stress concentration points which in turn gradually affect the stiffness of the peri-implant bone [26] compromising secondary implant stability and increasing the likelihood of failure. To overcome these limitations, previous studies have implemented overloading testing sequences where the screw is loaded and unloaded with increasing amplitude until failure [5,6,12,27,28]. This allows measuring the progressive stiffness degradation of the implant, as well as energy description and permanent deformation, parameters that are commonly used to define the loss of primary stability. These studies have shown that, for example, the stiffness of commonly used dental implants degrades progressively with each load cycle reaching an average of 30 % to 50 % degradation at the point of failure [12,27]. Furthermore, it has also been shown that an increase in energy dissipation and a reduction in stiffness can be noticed after imposing a displacement of 0.16 mm on these same implants [27]. Despite this, this same studies also point out that more work needs to be done to determine how much force can be applied to an implant right after implantation without compromising primary stability.

With this in mind, this study will investigate how cyclic overloading facilitates the progressive loss of primary implant stability of implanted osteosynthesis screws under three loading configurations, axial, shear, and mixed loading. To achieve this, a set of 2.5 mm locking osteosynthesis screws were implanted in bone samples harvested from porcine bones and tested using an in-house build test set-up which replicates the loading mechanism of implanted locking screws under cyclic overloading. Stiffness degradation, commonly referred to as damage, as well as dissipated energy were measured and used to determine a point where primary stability is seemingly lost. Furthermore, it was determined if the failure point defined using damage and dissipated energy resulted in permanent peri-implant deformation outside of the range of 50 to 150 μm which will mean that secondary implant stability is compromised for a particular screw.

The results of this study aim to provide a more comprehensive failure definition, which considers the critical loss of primary implant stability and the range of desirable micro motions needed to achieve secondary implant stability as well as how both of these vary among various loading configurations. This information will aid in surgical planning by providing insight on the impact of loading configurations on the holding capacity and failure of locking screws, which in turn can be used to optimize the implantation site selection.

2. Materials and methods

2.1. Summary

For this study, 30 samples harvested from fresh frozen porcine distal radii were used and separated into 3 groups (10 samples per group) depending on loading configuration: axial loading with 0° inclination, mixed loading with 45° inclination, and shear loading with 90° inclination. The loading was done using a specific overloading testing sequence which included 20 pre-containing cycles with load amplitude between 0 and 15 N, followed by cyclic loading with an increasing amplitude of 1 N per cycle returning to a base load of 15 N. The loading was applied as tension, meaning that the screws were pulled, not pushed. The screws were tested until failure, which was defined as screw pull-out for 0° and 45° loading, and the first cut-through event for 90° loading. Force and displacement data were recorded for each load cycle and used to calculate several failure indicators. The following sections will cover the main aspect of testing in more detail.

2.2. Sample harvesting and preparation

As mentioned above, the samples used for the present study were

harvested from porcine bones. this was done based on previous studies which show that pig bones are suitable replacements for human bones since they replicate the mechanical properties [13] and structural characteristics [29] of human bones.

With this in mind, the sample harvesting and preparation are as follows. First, a set of 30 distal radii were acquired from the local abattoir. The bones were then cleared of any soft tissue after which a 20 mm cylindrical sample was extracted from each bone in locations where human-like bone morphologies could be found, according to [29]. The selected samples closely resemble the *peri* implant bone morphology present around screws implanted closer to the articular surface while handling fractures of the distal radius. Samples were extracted using a conventional drill-press with a modified core driller which allowed to simultaneous drill a 2 mm pilot hole perfectly aligned and centered within the sample. The sample diameter was set to 20 mm to guarantee enough space between the area of relevant peri-implant strain distribution [11,27] and the edge of the sample while the pilot hole size was selected based on the screw manufacturer implantation guide. After harvesting the samples, a 2.5 mm locking screw (Medartis 2.5 locking screw; A-5750, Medartis Inc., Basel, Switzerland) was implanted using a universal mechanical testing machine (ZwickiLine Z2.5, ZwickRoell GmbH & Co. KG, Ulm, Germany) following the implantation procedure presented in [11] which consist of 20 N compressive force and rotation speed of 5 r.p.m.; this same machine was used for mechanical testing. Correct alignment between the machine axis, screw, and sample was controlled using two-line laser in two perpendicular positions and the insertion depth was kept constant at 15 mm for all samples, all screws were implanted mono cortically. Both the bones and the harvested samples (without screw) were kept frozen at −20 °C and left to thaw for 24 h at 4 °C prior to implantation and mechanical testing, Fig. 2 shows the harvesting and implantation experimental set-ups.

2.3. Mechanical testing

Samples were tested using an in-house build test set-up consisting of a screw clamp which replicates the locking mechanism between the screw and the osteosynthesis plate and a bottom jig which allows to test inclinations from 0 to 90° (with respect to the load application axis) and plate elevations between 0 and 2 mm (Fig. 3). All screws were tested using a cyclic overloading test sequence based on that presented in [30] with slight modifications made based on the difference in test subject (whole bone vs. single screw) and machine type (servo-hydraulic vs. quasi-static).

The implemented test sequence consisted of a pre-conditioning phase where the sample was subjected to 20 loading cycles oscillating between 0 and 15 N. After a 1-second pause, a cyclic overloading phase followed where the sample was loaded until failure in cycles where the amplitude was increased by 1 N per cycle while keeping a constant valley load of 15 N, both pre-conditioning and loading were done under force-controlled loading at a rate of 50 N/s, Fig. 4 shows a graphic representation of this information. Displacement of the screw clamp was measured using a linear variable differential transformer (LVDT) position sensor (Hottinger Baldwin Messtechnik GmbH, Darmstadt, Germany) placed as close as possible to the implantation site, this was done to account for the machine and test set-up compliance.

Failure was defined as the screw being completely pulled out from the bone samples for the axial and mixed load cases. For the shear load case, the screw does not get pulled from the bone entirely, instead cutting through the bone and progressively digging itself deeper into the sample before ultimately breaking. Since this failure happens at rather high deformations (>10 mm), failure was defined as the first cut-through event similar to how is done in [13] and [10] which for this study was identified as the first saddle point of the enveloping load vs. displacement curve represented by a dashed black line in Fig. 5. This loading sequence was selected over that presented in [12] and [27], studies that can be considered thematically close to this one, because it allows measuring the gradual change in relevant variables in smaller intervals, more continuous. Finally, stiffness was calculated as the secant line connecting the point of load application and load removal for each cycle (Fig. 6). The measured variables for every cycle ($c = 1$ to n) were kept the same as those reported in these studies and are defined herein as:

- Cycle displacement, ${}^{c}d_{\text{cycle}}$
- Maximum cycle displacement, ${}^{c}d_{\text{max}}$
- Failure displacement, d_{fail}
- Maximum cycle force, ${}^{c}F_{\text{max}}$
- Failure force, F_{fail}
- Cycle stiffness, ${}^{c}K$

using this data, the following values were calculated:

- Permanent displacement, ${}^{c}d_{\text{perm}} = \sum_{i=1}^{c} {}^{i}d_{\text{cycle}}$
- Damage, ${}^{c}D = 1 - {}^{c}K/{}^{1}K$
- Normalized displacement, ${}^{c}d_{\text{norm}} = {}^{c}\text{d}_{\text{max}}/\text{d}_{\text{fail}}$ (ranging from 0 to 1)
- Normalized Force, ${}^{c}\text{F}_{\text{norm}} = {}^{c}\text{F}_{\text{max}}/\text{F}_{\text{fail}}$ (ranging from 0 to 1)

The dissipated energy (${}^{c}E$) was calculated numerically as the area under the force vs. displacement curve for every cycle. Finally, while stiffnesses for both the loading and unloading were calculated using the secant line of each portion, only the results regarding the loading portion of the cycle are referenced throughout this study, this was done following the procedures presented in [12,26]. Fig. 6 shows a graphical representation of these values calculated for 3 cycles for ease of understanding.

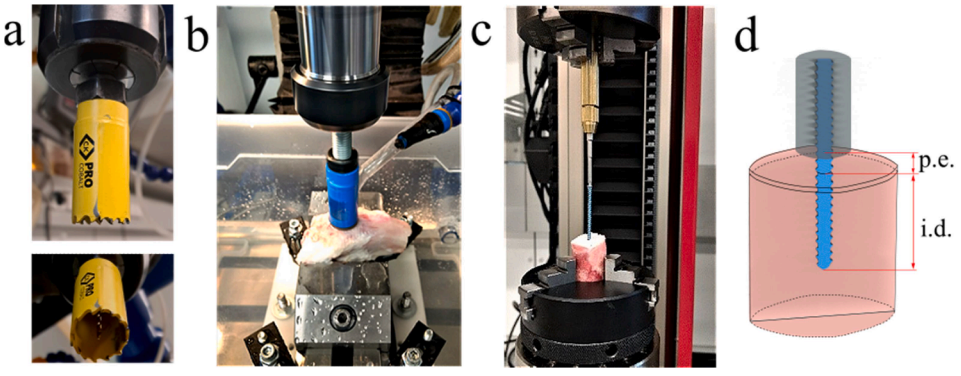

Fig. 2. Sample preparation protocol containing a) sample extraction tool. b) water cooled drilling procedure. c) Controlled screw implantation. d) sample schematic showing plate elevation (p.e.) and implantation depth(i.d.), the area shaded in grey represents the clamping region.

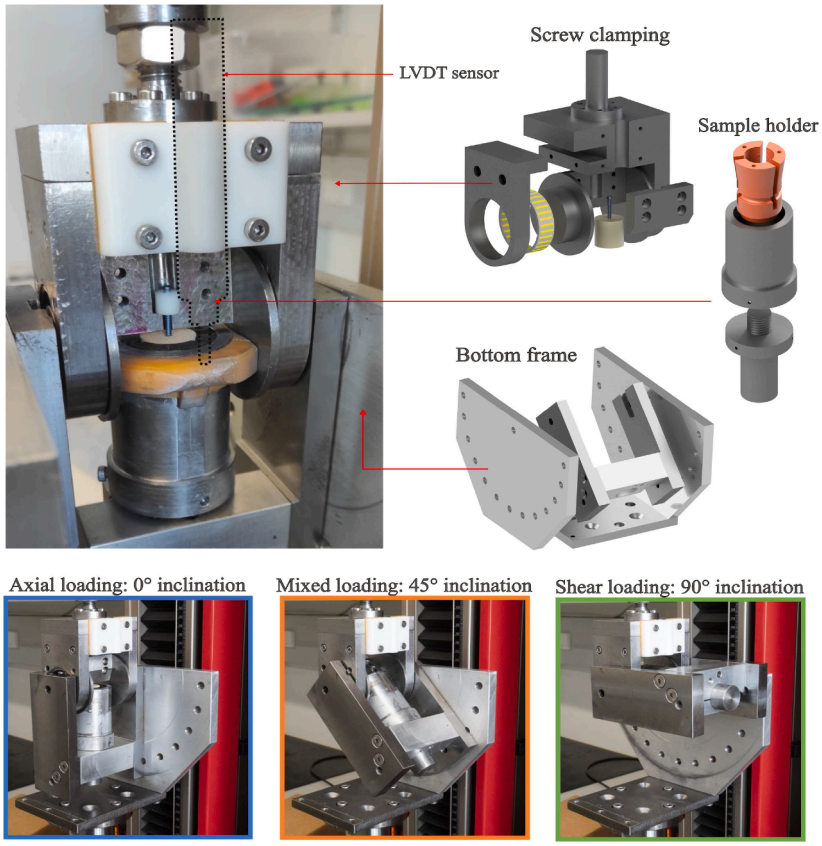

Fig. 3. Experimental test set-up. From top to bottom view of test set-up with sample mounted and 3D renderings of the individual components. LVDT sensor was removed to reveal inner working of the set-up but is outlined by a dashed line, set-up inclination for every test, isometric.

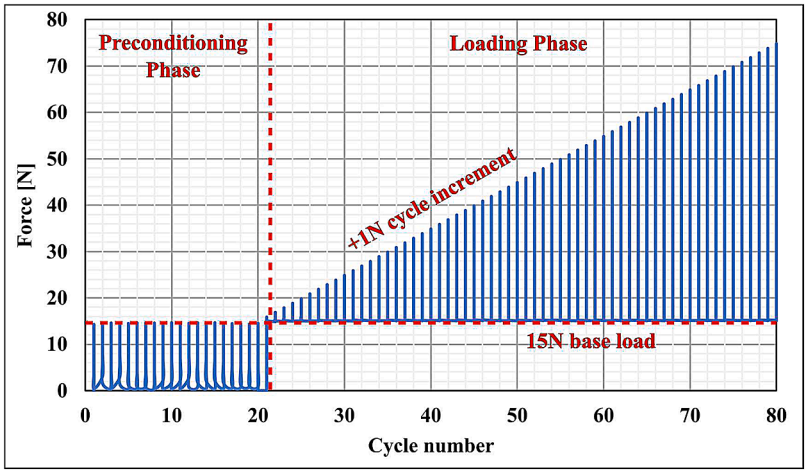

Fig. 4. Schematic representation of the implemented test-sequence.

2.4. Data processing and statistical analysis

Critical loss of primary implant stability was determined using ${}^{c}E$ and ${}^{c}D$ following a similar procedure to that presented in [27] where similar size screws were tested using a cyclic overloading method where the displacement amplitude was increased stepwise, starting at 0.04 mm (${}^{c}d_{norm} = 0.03125$), and increasing to 0.08, 0.16, 0.32, 0.64 and 1.28 mm (${}^{c}d_{norm} = 1$).

For this, the ${}^{c}E$ and ${}^{c}D$ values measured at "probing-points" corresponding to ${}^{c}d_{norm} = 0.03125$, 0.0625, 0.125, 0.25, 0.5 and 1 were averaged among the 10 samples of each load case. Afterwards, the limit for primary implant stability definition was done by determining at which ${}^{c}d_{norm}$ probing-point both ${}^{c}E$ and ${}^{c}D$ show a statistically significant increment with respect to the same variables measured at the first load cycle (here on referred to as ${}^{c}d_{n}=0$ or 0 for convenience). Kruskal-Wallis comparison tests were used to identify significant differences in both ${}^{c}E$ and ${}^{c}D$ at the different displacement levels ($\alpha=0.05$). This was done in order to compare the results of this study to those presented in previous studies, particularly those presented in [4,6,12,26,27]. All data processing was done using in-house build Python scripts and Microsoft Excel (r2022). Non-parametric statistical analysis was done using XLSTAT for Microsoft Excel (r2022, Addinsoft SARL, New York, NY,

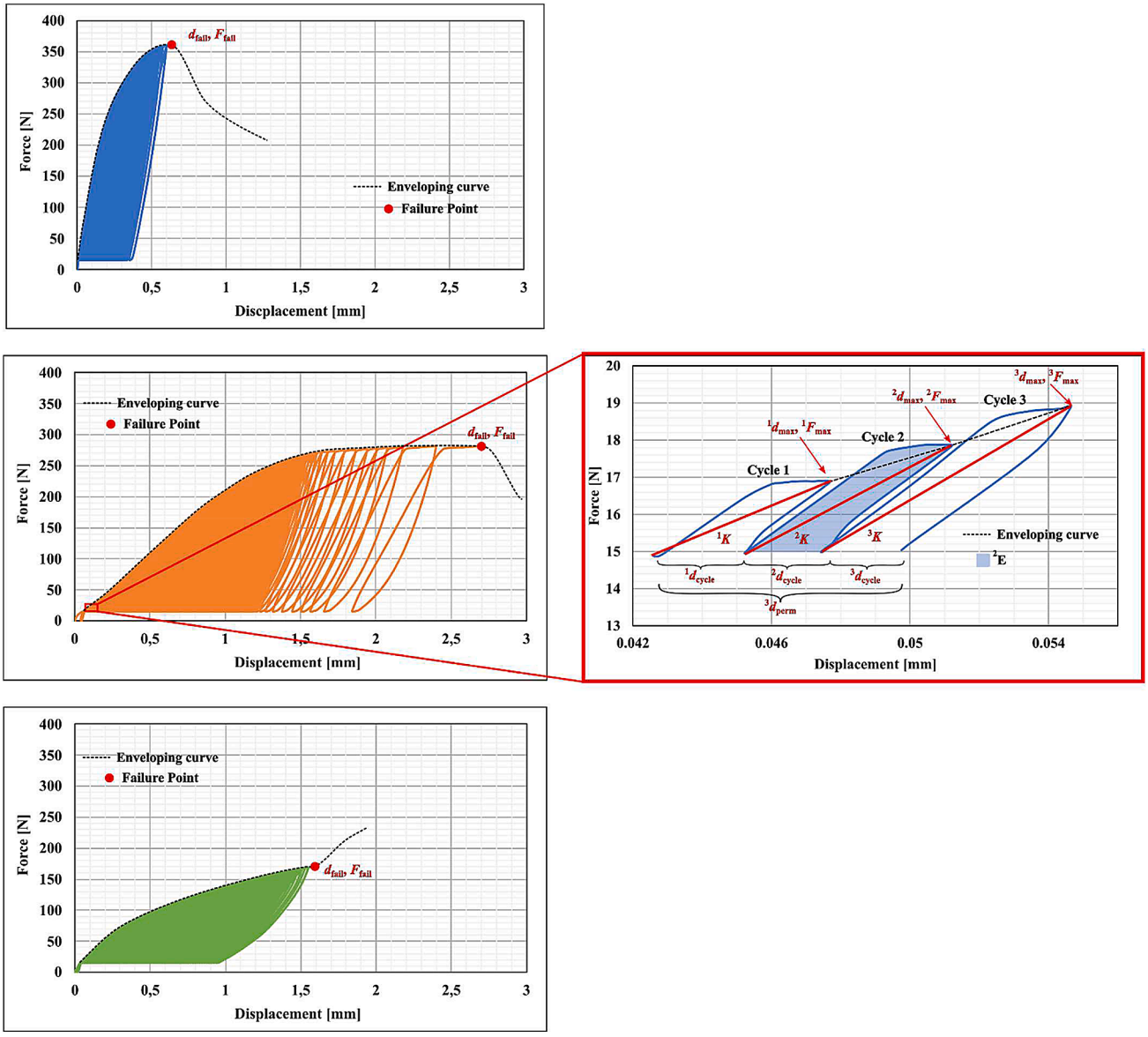

Fig. 5. Measured and calculated variables for all load cases. Cycles specific calculation (Right side) shown only for the mixed loading load case for simplicity.

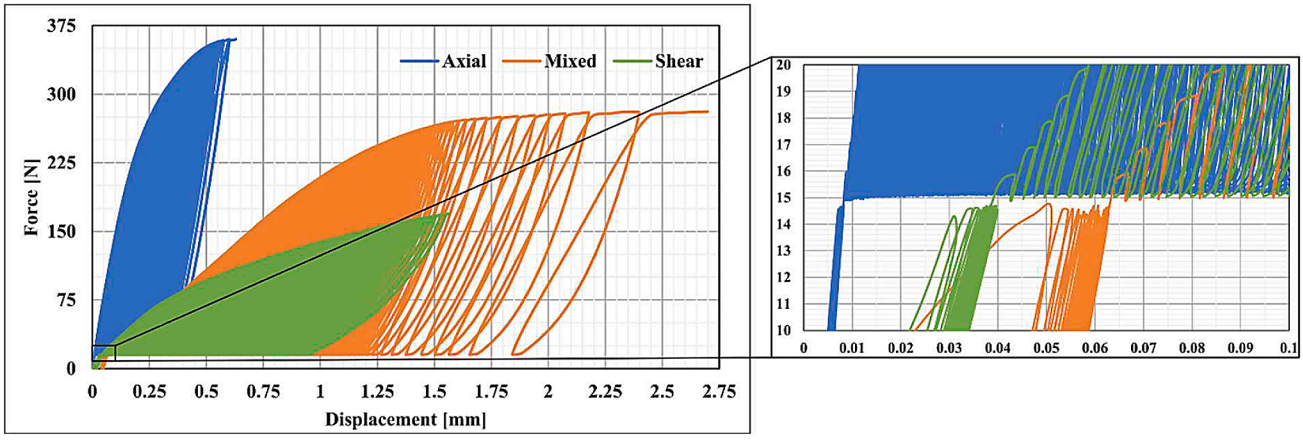

Fig. 6. Load vs. Displacement curves for the tested load cases, axial lading in blue, mixed loading in orange and shear loading in green. This colour scheme was kept throughout the study.

USA). Linear and non-linear regression analyses where performed using the same software and, unless expressed otherwise, all presented correlation values have a significance level of $p < 0.001$.

3. Results

3.1. Mechanical testing

Typical load vs. displacement curves for the three tested load cases can be seen in the following figure which shows that permanent displacement deformation occurs as early as the first load cycle for all load cases (Fig. 6).

Average values for failure forces, displacements, permanent deformations, initial stiffnesses and final damage values are presented in the following table.

Significant differences (p values marked as <0.05 in Table 2 were found between all the measurements presented above with the exception of failure force (F_{fail}) between axial and mixed loading, initial stiffness (^1K) between mixed and shear loading, and final damage (^nD) between shear and mixed loading as well as shear and axial loading. Similar behaviors were observed between initial stiffness (^1K) and failure forces (F_{fail}), with the highest value for both measurements observed in the mixed loading case, followed by axial loading and shear loading presenting the lowest measured mean values.

Despite this, very poor correlations ($R^2<0.3$) were found between initial stiffness (^1K) and failure forces (F_{fail}) for all load cases which implies that stiffer samples are not necessarily those with higher failure forces. Similar results were observed for comparisons between initial stiffness (^1K), failure displacement (d_{fail}), permanent deformation ($^nd_{perm}$), and final damage (^nD) with the exception of damage and initial stiffness for mixed and shear loading which show a moderate and strong correlation respectively which indicates that initial stiffness is not an ideal predictor of any potential failure metric. This can be better seen in the Fig. 7.

3.2. Permanent deformation, damage, and energy dissipation evolution

Fig. 8 depicts the average cycle displacement ($^cd_{cycle}$) and ($^cd_{norm}$) among the 10 samples tested in all load cases: axial, mixed, and shear. In the axial loading case, the $^cd_{cycle}$ increases in an exponential manner, starting at 0.1 μm and stabilizing at around 9 μm on average. Similarly, in the mixed loading case, $^cd_{cycle}$ also increases exponentially, however, the initial and final values are notably higher, at 1 μm and 27 μm, respectively. Finally, the shear loading case shows a slower exponential increase in average $^cd_{cycle}$ as $^cd_{norm}$ starting at 3 μm and reaching a final

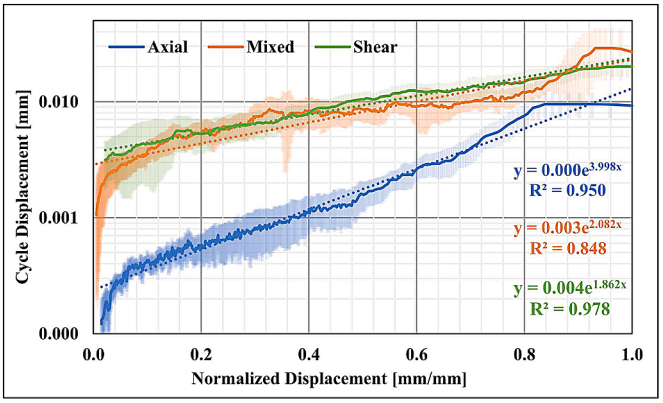

Fig. 8. Cycle displacement vs. Normalized maximum displacement. Exponential trend lines shown as dashed lines for every load case as well as correlation values.

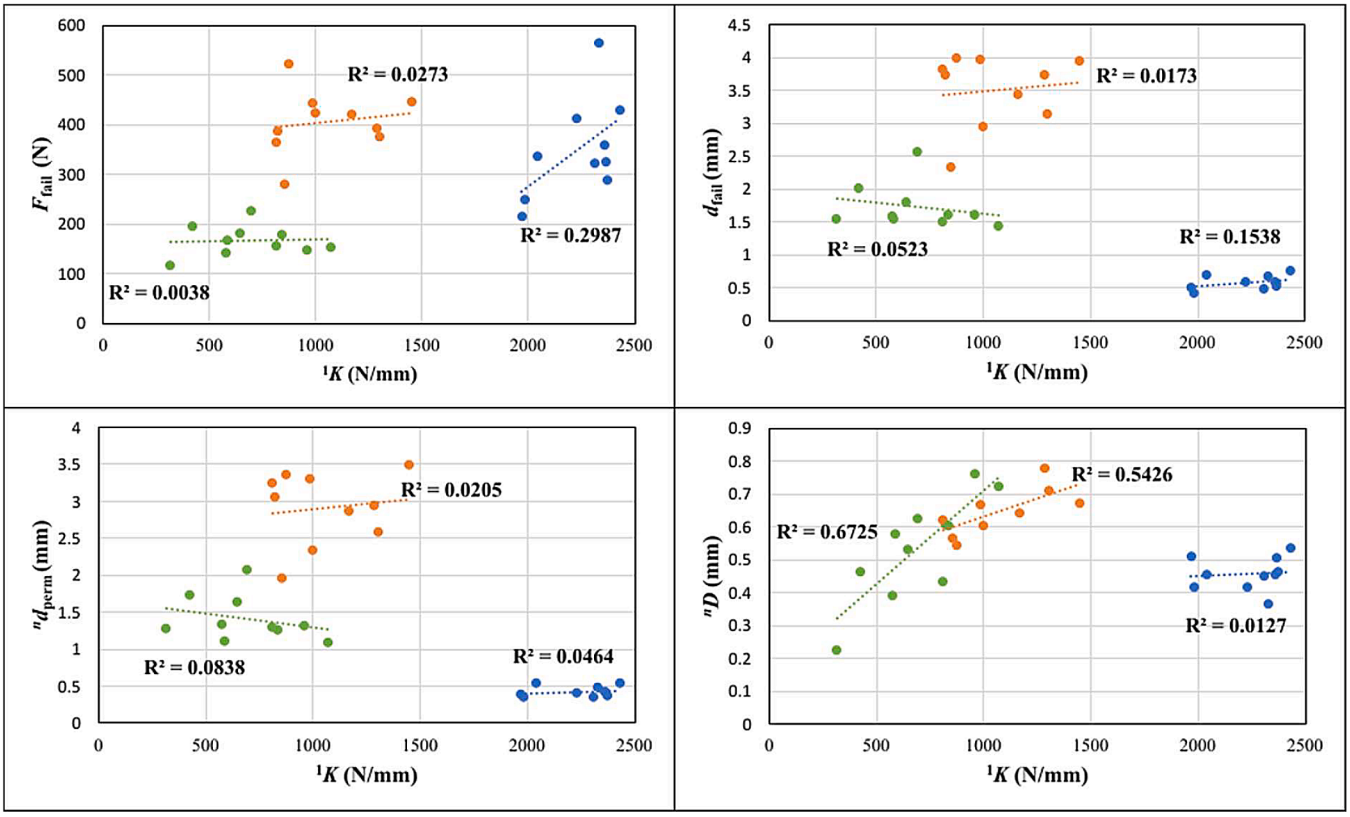

Fig. 7. Scatter plots showing the relationships between initial stiffness and Failure force (top left), Failure displacement (top right), Permanent deformation (bottom left), and damage (bottom right).

value of 20 μm. The exact correlation values can be seen on the figures for each load case.

The non-zero initial ${}^{c}d_{cycle}$ in these cases suggests that, although small, the sample undergoes permanent deformation from the very beginning of the loading phase. This can be observed in Fig. 9, which shows that ${}^{c}d_{perm}$ and ${}^{c}d_{norm}$ are related by a linear function, starting at initial values of 7 μm, 16 μm, and 3 μm for the axial, mixed, and shear loading cases, respectively.

As the applied load always leads to permanent deformation, a failure point based on the elastic limit, similar to yielding in continuous materials, cannot be established for the tested load cases. However, for implanted load screws, early-stage permanent displacement does not necessarily imply significant loss of functionality as the screws have the capability to withstand higher loads before reaching failure points such as pull-out or cut-through, as shown in Fig. 6. A more accurate assessment of loss of functionality can be determined by analyzing damage (${}^{c}D$) and dissipated energy (${}^{c}E$) per cycle, as shown in Figs. 10 and 11. Final damage (${}^{n}D$), as shown in Table 1, indicate the degree to which the initial stiffness of the samples has been degraded as a result of the applied load. Fig. 11 illustrates the progression of ${}^{c}D$ throughout the loading phase for all load cases, and in general, it correlates well with the ${}^{c}d_{n}$ via a power relationship. From the figure, it can also be estimated, albeit mostly qualitatively, the rate at which stiffness degradation occurs for each load case. For the axial loading case, the ${}^{c}D$ progression is proportional to the normalized displacement (${}^{c}d_{norm}$), with approximately 50 % of the final stiffness degradation happening slightly below half of the normalized displacement (${}^{c}d_{norm}$ ~0.46). In contrast, the screws tested under mixed and shear loading show a much higher ${}^{c}D$ rate at the beginning of the loading phase, with 50 % of the final stiffness degradation occurring at 14 % of the ${}^{c}d_{norm}$ for the mixed loading case and 11.5 % for the shear loading case.

For all load cases, a power-law relationship was found between dissipated energy (${}^{c}E$) and normalized displacement (${}^{c}d_{norm}$) (Fig. 11). The axial loading case had the lowest average ${}^{c}E$ on the first cycle at 0.003 mJ, followed by mixed loading at 0.022 mJ and 0.064 mJ. By the end of the test phase, the samples tested under the mixed loading case had the highest average ${}^{c}E$ of 94.78 mJ and an average total energy dissipation of 8660.2 mJ. The axial loading case had the second-highest values, with an average final ${}^{c}E$ of 25.19 mJ and an average total energy dissipation of 1337.03 mJ. The screws tested under shear loading had the lowest values for both final ${}^{c}E$ and total energy dissipation, at 13.57 mJ and 886.51 mJ, respectively.

For all load cases, it was showed that average damage (${}^{c}D$) and dissipated energy (${}^{c}E$) at normalized displacement (${}^{c}d_{norm}$) values of 0.0325 and 0.0625 were not significantly different that those measured at the first load cycle (${}^{c}d_{norm} = 0$) with significant differences appearing only after ${}^{c}d_{norm} = 0.125$ for both measurements in every load case

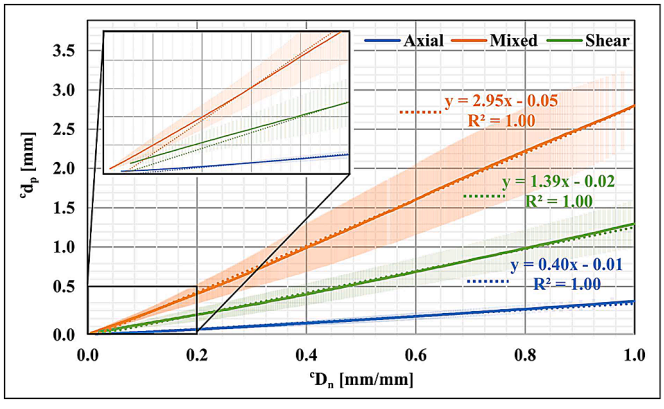

Fig. 9. Linear relationship between permanent deformation and normalized maximum displacement.

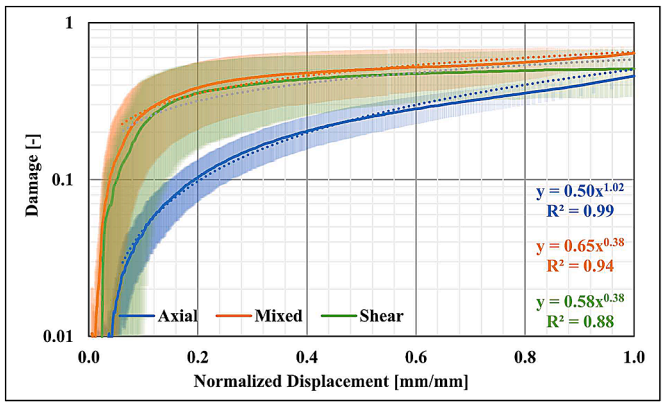

Fig. 10. Damage evolution as a function of the maximum normalized displacement. Logarithmic scale was chosen to better visualize the initial damage evolution.

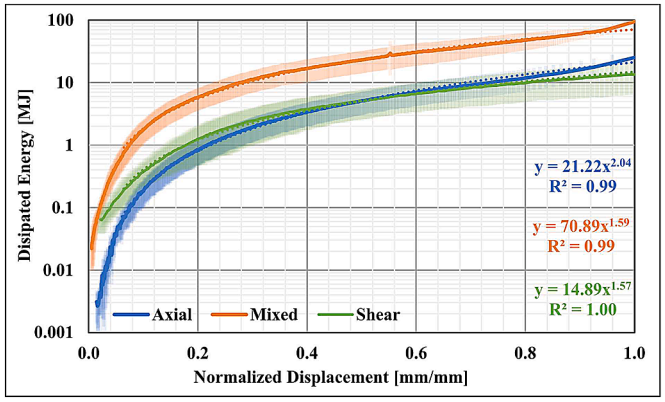

Fig. 11. Dissipated energy evolution as a function of the maximum normalized displacement. Logarithmic scale was chosen to better visualize the initial energy dissipation evolution.

Table 1
Average failure force and displacements recorder for every load case as well as calculated damage and initial stiffness, maximum and minimum values showed in parentheses.

	Axial loading	Mixed loading	a) Shear loading
F_{fail} (N)	350.45±99.79 (215.88–563.81)	460.03 ± 63.63 (280.88–523.92)	166.85 ± 30.36 (116.88–225.92)
d_{fail} (mm)	0.58±0.10 (0.43–0.76)	3.51 ± 0.55 (2.33–3.99)	1.73 ± 0.34 (1.43–2.58)
${}^{n}d_{perm}$ (mm)	0.43±0.07 (0.34–0.54)	2.91 ± 0.49 (1.95–3.48)	1.41 ± 0.31 (1.08–2.07)
${}^{n}D$ (-)	0.46±0.05 (0.37–0.53)	0.64 ± 0.07 (0.54–0.78)	0.53 ± 0.16 (0.22–0.76)
^{1}K (N/mm)	2238.74±174.78 (853.09–1968.39)	1054.45 ± 230.32 (811.10–1449.38)	692.89 ± 235.78 (315.92–1072.92)

(Table 3). This means that at a ${}^{c}d_{norm}$ equal to 0.125, a critical loss of primary implant stability marked by a significant increase in both ${}^{c}D$ and ${}^{c}E$ can be observed. Therefore, a ${}^{c}d_{norm}$ value equal to 0.0625 can be considered the limit for primary implant stability.

3.3. Permanent deformation and ideal range of micro-motions

Upon identifying the failure point using critical ${}^{c}D$ and ${}^{c}E$ values as criteria, it was crucial to examine whether this failure point aligns with the peri-implant micromotion range required for secondary stability. Specifically, it was important to confirm that the critical values of

Table 2
p-values for all comparisons made. P-values greater than 0.05 are emphasized in the table for the sake of clarity.

	F_{fail} (N)			d_{fail} (mm)			${}^{n}d_{perm}$ (mm)			${}^{n}D$ (-)			${}^{1}K$ (N/mm)		
	Axial	Mixed	Shear	Axial	Mixed	Shear	Axial	Mixed	Shear	Axial	Mixed	Shear	Axial	Mixed	Shear
Axial	1.00	**0.23**	<0.05	1.00	<0.05	<0.05	1.00	<0.05	<0.05	1.00	<0.05	**0.09**	1.00	<0.05	<0.05
Mixed		1.00	<0.05		1.00	<0.05		1.00	<0.05		1.00	**0.06**		1.00	**0.05**
Shear			1.00			1.00			1.00			1.00			1.00

Table 3
Calculated p-values between the different probing stages. significant levels are indicated by (*).

p-values calculated for ${}^{c}E$							
${}^{c}d_{norm}$	**<0.001**	**0.036**	**0.062**	**0.125**	**0.250**	**0.500**	**1.000**
0 (Axial)	–	0.455	0.053	0.002*	<0.001	<0.001	<0.001
0 (Mixed)	–	0.267	0.056	0.001*	<0.001	<0.001	<0.001
0 (Shear)	–	0.496	0.067	0.002*	<0.001	<0.001	<0.001
p-values calculated for ${}^{c}D$							
${}^{c}d_{norm}$	**<0.001**	**0.036**	**0.062**	**0.125**	**0.250**	**0.500**	**1.000**
0 (Axial)	–	1.000	0.259	0.003*	0.003*	0.003*	0.003*
0 (Mixed)	–	0.320	0.057	0.002*	<0.001	<0.001	<0.001
0 (Shear)	–	0.875	0.917	0.003*	0.003*	0.003*	0.003*

maximum allowed permanent displacement (${}^{c}d_{perm}$) established earlier resulted in peri-implant deformation within the range of 50 to 150 μm, which promotes osseointegration (ideal scenario), below 50 μm, which does not promote osseointegration but still provides adequate stability during fracture healing (less than ideal but acceptable), or above 150 μm, which leads to compromised secondary stability and further complications (not ideal). Table 4 shows the average maximum cycle displacement (${}^{c}d_{max}$), maximum cycle force (${}^{c}F_{max}$), and permanent displacement (${}^{c}d_{perm}$) for all load cases at the defined level of critical normalized displacement (${}^{c}d_{norm}$) value (0.625) and the following level (0.0125), displacements are shown in micrometers (μm) to better interpret the results.

Permanent cycle deformation (${}^{c}d_{perm}$) in the critical normalized displacement (${}^{c}d_{norm}$) value (0.0625) followed the same trend as those seen in the results presented above with mixed loading having higher values, followed by shear loading and axial loading showing the lowest values. Screws tested under axial loading presented ${}^{c}d_{perm}$ values below the lower limit of the desired micromotion range for both at ${}^{c}d_{norm}$ = 0.0625 and 0.125. Screws tested under shear loading were the only ones to present average ${}^{c}d_{perm}$ completely withing the desired range of micromotions at the limit value while screw tested under mixed loading showed average ${}^{c}d_{perm}$ values slightly above the desired range. Screws tested under both mixed and shear loading showed average ${}^{c}d_{perm}$ values higher than the upper limit of the ideal micromotions range at 12.5 % of final maximum deformation.

Additionally, at a value of ${}^{c}d_{norm}$ equal to 0.0625, the maximum cycle force (${}^{c}F_{max}$) was approximately 20 % of the recorder (F_{fail}), with values of 19.33 %, 19.80 %, and 18.43 % for axial, mixed, and shear loading, respectively. These results suggest that 20 % of the failure force, regardless of it being pull-out or cut-through force, can be used as a limit for primary implant stability under the loading configurations tested in this study.

4. Discussion

The goal of this study was to identify a point at which an implanted osteosynthesis screwloses its functionality under three loading configurations: axial, mixed, and shear loading. To do this, an in-house test setup and overloading test sequence were used to measure yielding estimators, such as damage (${}^{c}D$), permanent deformation (${}^{c}d_{perm}$), and energy dissipation (${}^{c}E$). These measurements were used to define a critical loading value at which primary implant stability is lost, thus compromising the screw's functionality. The results of this study can be useful for surgeons in determining optimal screw implantation sites based on local bone morphology or as a post-operative guide for determining how much load can be safely placed on the implant. In the following sections the obtained results will be discussed in more detail in the same order as they were presented in the results section.

4.1. Mechanical testing

Previous studies have tested osteosynthesis screws and screw-like implants under similar conditions to the ones presented here. However, direct comparison between the results presented here and those from preceding works might not be completely useful since failure loads and displacements depend on several factors including screw type, peri-implant bone morphology, sample provenance and implantation technique.

Pull-out and cut-through forces for screws tested under axial and shear loading were in the same order of magnitude of those presented in [13] where 2.7 mm head locking screws were tested on porcine bones and recorder failure forces (F_{fail}) of 744±185 N and 431±155 N for axial and shear loading, respectively. In contrast, both axial and shear stiffness presented here were almost twice as high compared to those presented in this same study (axial stiffness = 309 ± 88 N/mm, shear stiffness = 305 ± 83 N/mm), this can be due to many factors including the sample provenance (cuboid vs. radius) and test up but also implantation technique. Another study [31] uses experimental and

Table 4
Forces, displacements, and permanent deformations for every load case at two probing levels, ${}^{c}d_{n}$ =0.0625 and 0.125.

	${}^{c}d_{norm} = 0.0625$			${}^{c}d_{norm} = 0.125$		
	${}^{c}F_{max}$ [N]	${}^{c}d_{max}$ [μm]	${}^{c}d_{perm}$ [μm]	${}^{c}F_{max}$ [N]	${}^{c}d_{max}$ [μm]	${}^{c}d_{pern}$ [μm]
i)Axial	64.78 ± 14.22	40.0 ± 6.2	19.7 ± 3.0	120.86 ± 30.90	72.2 ± 12.1	42.5 ± 8.8
a.Mixed	78.61 ± 10.10	220.5 ± 40.8	157.8 ± 38.4	126.79 ± 17.99	64.5 ± 114.3	330.8 ± 68.5
Shear	30.10 ± 2.79	110.7 ± 41.8	89.3 ± 30.3	46.49 ± 6.01	0.231.3 ± 82.4	177.1 ± 64.5

non-linear finite element analysis to calculate the axial stiffness of dental implants tested under similar loading conditions as those presented here. In this study comparable stiffness ranges (1180 to 3050 N/mm) with the average axial stiffness values presented here being slightly lower. Finally, a similar test set-up was used in [32] to test implanted screws on two different load cases, axial compression, and shear loading. Compared to the results presented here, axial stiffness is noticeably lower with average values around 2600 N/mm (Table 1) compared to stiffness values around 4300–4400 N/mm which can be due to the difference in loading direction (compression vs. tension). Shear stiffness on the other hand presents comparable values in both studies with ours being 200–300 N/mm lower on average.

4.2. Permanent deformation, damage, and energy dissipation evolution

Subjecting samples to cyclic overloading allow the investigation of the progressive stiffness degradation or damage of the bone-screw interface which ultimately leads to screw loosening and failure. Earlier studies on the subject have shown that at the point of failure dental implants with a diameter of 3.5 mm experience between 30 and 40 % stiffness degradation [12,27]. The results presented here show that 2.5 mm locking osteosynthesis screws subjected to a similar overloading test sequence experience damage levels in the same order of magnitude, albeit higher that the ones presented in said studies with average damage value ranging between 46 and 64 %.

For the sake of comparison, the measured maximum cycle displacement (${}^{c}d_{\max}$) was normalized by dividing it over the maximum displacement at the last load cycle (d_{fail}). This allowed to better compare the results presented here to those presented in studies with closely related aims and results [12,27]. Non-parametric statistical comparison tests were carried out between the average damage (${}^{c}D$) and (${}^{c}E$) values at the aforementioned normalized displacement (${}^{c}d_{\text{norm}}$) probing points and it was found that for the tested load cases at an imposed displacement of ${}^{c}d_{\text{norm}} = 0.125$ a significant increase in both ${}^{c}D$ and ${}^{c}E$ can be observed. These values correspond to ~0.04 mm, ~0.22 mm, and ~0.11 mm of applied displacement for axial, mixed, and shear loading, respectively. These results are comparable to those presented in [27] where a significant increment for these same variables was observed between measurements made at ${}^{c}d_{\text{norm}} = 0.125$ and 0.25 thus suggesting ${}^{c}d_{\text{norm}} = 0.125$ (0.16 mm) as the point where initial stability significantly deteriorates. The differences in values can potentially be attributed to the type of implant and load direction (compression vs. tension) tested.

Previous studies have shown that peri-implant damage occurs relatively close to the screw implant interface with high strain values present closer to the screw outer diameter [1,6,27,32]. While the results presented in this study might not be enough to corroborate this information, they suggest that permanent displacement (${}^{c}d_{\text{perm}}$), damage (${}^{c}D$), and dissipated energy (${}^{c}E$) occur from the very first loading cycle, even at small displacement amplitudes. This finding is interesting as it suggests that tissue closest to the bone-screw interface may contribute the most to screw failure, as it experiences micro motions leading to mechanical degradation from the first cycle, despite the fact that some level of micro motions is beneficial for implant success. Further studies exploring the bone-screw interface using the same implant and loading protocols could shed more light on this topic.

4.3. Failure definitions: yielding, loss of function, and ultimate failure

The results of this study indicate that yield-like behavior, or permanent deformation product of an applied load, is present from the first load cycle, despite no visible loss of functionality. Significantly higher ${}^{c}E$ and ${}^{c}D$ occur at a normalized displacement level of ${}^{c}d_{\text{norm}} = 0.125$ of maximum displacement for all load cases, similar to that presented in previous studies. This suggests that a ${}^{c}d_{\text{norm}} = 0.0625$ can be considered the limit for the safe operation of an implanted bone screw. Furthermore, at the same level, all load cases present ${}^{c}d_{\text{perm}}$ values that can be considered safe since they fall below or within the range of 50 to 150 micrometers. At the following displacement level (${}^{c}d_{\text{norm}} = 0.125$), two load cases present ${}^{c}d_{\text{perm}}$ values higher than the desired range of micromotions, which can indicate a point where the screw is loosened, and secondary stability may not be achieved.

It is worth noting that, for the case of axial loading, ${}^{c}d_{\text{perm}}$ was not found to be over the range of micro motions at ${}^{c}d_{\text{norm}} = 0.625$ or 0.125, meaning that despite showing significantly higher damage and energy dissipation at 12.5 % of the failure displacement (d_{fail}), the screw's peri-implant motions might still lead to secondary implant stability. Despite this, studies show that screws are subjected to combined loads [15,16], which means that this assumption may not be entirely safe.

Finally, this study shows that loss of functionality occurs consistently at around 20 % of F_{fail} in all load cases. Since it is usual to define implant failure force in terms of pre- and post-operative estimators [12], the definition presented here can also be achieved by these means. This aids the development of tools for surgery planning that account for both primary and secondary stability which can prove useful for surgeons during surgery planning. With these results in mind, failure of implanted osteosynthesis screws can be separated into three stages: 1. Yielding, meaning permanent deformation of the screw-bone interface which occurs as soon as the implant is loaded, 2. Loss of primary stability, meaning that the screw has lost its functionality marked by a significant increase in both ${}^{c}D$ and ${}^{c}E$ occurring consistently at 20 % of the F_{fail}, the point at which the screw is either pulled from the bone or it has cut through it.

4.4. Limitations

The present study has some limitations that must be considered when interpreting the findings. Firstly, the use of animal models in this study might not necessarily reflect the wide spectrum of human bone morphologies where the selected screws are commonly implanted. This limits the generalizability of the findings and suggests that further studies in human cadavers or potentially clinical trials could help confirm the results. Furthermore, our results and derived conclusions can only be considered valid for 2.5 mm osteosynthesis screws implanted mono cortically. Therefore, it is necessary to exert caution if the findings of this work are to be applied to another screw size and placement (for example, bi cortical implantation).

Another limitation of this study is that it is limited to three load cases (axial, shear, and combined loading) and does not include compressive tests, which might not cover the whole range of anatomical loading. This means that the results of this study should be considered in the context of the loading conditions tested and should not be extrapolated to other types of loading scenarios.

Furthermore, the point of loss of primary stability is defined based on the failure point, which means that it is necessary to know when the screw will fail to determine when primary stability was lost. This calls for the development of better pre-operative or pre-implantation prediction tools to accurately determine the point of stability loss. This is important in order to optimize implantation technique, improve surgical outcomes and reduce the risk of complications.

Finally, it was defined that ${}^{c}d_{\text{norm}} = 0.125$ was the maximum displacement that could be applied before compromising secondary implant stability. This is a consequence of the way in which data measurement was discretized (${}^{c}d_{\text{norm}}$=0.03125, 0.0625, 0.125, etc.) which means that an imposed displacement of ${}^{c}d_{\text{norm}}$=0.125 does not necessarily represent the exact point of failure.

5. Conclusions

In conclusion, the goal of this study was to identify a point at which an implanted osteosynthesis screw loses its functionality under three loading configurations: axial, mixed, and shear loading. The results obtained here were used to measure plasticity estimators, such as

damage, permanent deformation, and energy dissipation. These measurements were used to define a critical loading value at which primary implant stability is lost, thus compromising the screw's functionality. The results of this study can be useful for surgeons in determining optimal screw implantation sites based on local bone morphology or as a pre-operative guide for determining how much load can be safely placed on the implant. The results of this study show that at an imposed load of 20 % of the failure force a significant increase in both damage and energy dissipation could be observed, which corresponds to a point where initial stability significantly deteriorates, at this same level, permanent deformation of the bone-screw interface is shown to be either within or below the range of micromotions widely regarded as safe. Additionally, it was found that permanent deformation, damage, and energy dissipation occur from the very first loading cycle, suggesting that the mechanical properties of the tissue closest to the bone-screw interface deteriorate from the very first load cycle and thus contribute significantly to the failure of the implant. These findings were consistent for the three loading configurations and could be supported by published works on the subject.

Funding

This project was funded by the Gesellschaft fr Forschungsfrderung Niedersterreich m.b.H. Life Science Call 2017 Grant No. LS17-004 and Science call 2019 Dissertationen Grant No. SC19-014.

Ethical approval

Not required.

Declaration of generative AI and AI-assisted technologies in the writing process

During the preparation of this work the author(s) used chatGPT strictly for the purpose of improving grammar and readability. After using this tool/service, the author(s) reviewed and edited the content as needed and take(s) full responsibility for the content of the publication.

CRediT authorship contribution statement

Juan D. Silva-Henao: Conceptualization, Methodology, Validation, Formal analysis, Investigation, Data curation, Writing – original draft, Visualization, Funding acquisition. **Sophie Schober:** Resources. **Dieter H. Pahr:** Conceptualization, Methodology, Resources, Writing – review & editing, Supervision, Funding acquisition. **Andreas G. Reisinger:** Conceptualization, Methodology, Resources, Writing – review & editing, Supervision, Project administration, Funding acquisition.

Declaration of competing interest

None declared.

Acknowledgements

The authors declare no conflict of interest related to this study. This project was funded by the Gesellschaft fuer Forschungsfoerderung Niederoesterreich m.b.H. Life Science Call 2017 Grant No. LS17004 and Science call 2019 Dissertationen Grant No. SC19014. No ethical approval was required for this study.

References

[1] Steiner JA, Ferguson SJ, van Lenthe GH. Computational analysis of primary implant stability in trabecular bone. J Biomech 2015. https://doi.org/10.1016/j.jbiomech.2014.12.008.

[2] Goharian A. Osseointegration Concepts of Trauma Fracture Fixation and Joint Replacement. Osseointegration of Orthopaedic Implants 2019:55–76. https://doi.org/10.1016/B978-0-12-813384-2.00003-5.

[3] Lioubavina-Hack N, Lang NP, Karring T. Significance of primary stability for osseointegration of dental implants. Clin Oral Implants Res 2006;17:244–50. https://doi.org/10.1111/J.1600-0501.2005.01201.X.

[4] Szmukler-Moncler S., Salama H., Reingewirtz Y., Dubruille J.H. Timing of Loading and Effect of Micromotion on Bone-Dental Implant Interface: review of Experimental Literature n.d. 10.1002/(SICI)1097-4636(199822)43:2.

[5] Joffre T, Isaksson P, Procter P, Persson C. Trabecular deformations during screw pull-out: a micro-CT study of lapine bone. Biomech Model Mechanobiol 2017;16:1349–59. https://doi.org/10.1007/S10237-017-0891-9/FIGURES/9.

[6] le Cann S, Tudisco E, Tägil M, Hall SA, Isaksson H. Bone Damage Evolution Around Integrated Metal Screws Using X-Ray Tomography — In situ Pullout and Digital Volume Correlation. Front Bioeng Biotechnol 2020;8:934. https://doi.org/10.3389/FBIOE.2020.00934/BIBTEX.

[7] Wirth AJ, Goldhahn J, Flaig C, Arbenz P, Müller R, van Lenthe GH. Implant stability is affected by local bone microstructural quality. Bone 2011;49:473–8. https://doi.org/10.1016/J.BONE.2011.05.001.

[8] Poukalova M, Yakacki CM, Guldberg RE, Lin A, Saing M, Gillogly SD, et al. Pullout strength of suture anchors: effect of mechanical properties of trabecular bone. J Biomech 2010;43:1138–45. https://doi.org/10.1016/J.JBIOMECH.2009.12.007.

[9] Tingart MJ, Lehtinen J, Zurakowski D, Warner JJP, Apreleva M. Proximal humeral fractures: regional differences in bone mineral density of the humeral head affect the fixation strength of cancellous screws. J Shoulder Elbow Surg 2006;15:620–4. https://doi.org/10.1016/J.JSE.2005.09.007.

[10] Seebeck J, Goldhahn J, Städele H, Messmer P, Morlock MM, Schneider E. Effect of cortical thickness and cancellous bone density on the holding strength of internal fixator screws. J. Orthopaedic Research 2004;22:1237–42. https://doi.org/10.1016/J.ORTHRES.2004.04.001.

[11] Ovesy M, Silva-Henao JD, Fletcher JWA, Gueorguiev B, Zysset PK, Varga P. Non-linear explicit micro-FE models accurately predict axial pull-out force of cortical screws in human tibial cortical bone. J Mech Behav Biomed Mater 2022;126:105002. https://doi.org/10.1016/J.JMBBM.2021.105002.

[12] Voumard B, Maquer G, Heuberger P, Zysset PK, Wolfram U. Peroperative estimation of bone quality and primary dental implant stability. J Mech Behav Biomed Mater 2019;92:24–32. https://doi.org/10.1016/J.JMBBM.2018.12.035.

[13] Lenz M, Gueorguiev B, Garces JBG, Swords MP, Rammelt S, Hofmann GO, et al. Axial and shear pullout forces of composite, porcine and human metatarsal and cuboid bones. J Orthop Translat 2018;14:67–73. https://doi.org/10.1016/J.JOT.2018.06.001.

[14] Panagiotopoulou VC, Ovesy M, Gueorguiev B, Richards RG, Zysset P, Varga P. Experimental and numerical investigation of secondary screw perforation in the human proximal humerus. J Mech Behav Biomed Mater 2021;116:104344. https://doi.org/10.1016/J.JMBBM.2021.104344.

[15] Synek A, Chevalier Y, Baumbach SF, Pahr DH. The influence of bone density and anisotropy in finite element models of distal radius fracture osteosynthesis: evaluations and comparison to experiments. J Biomech 2015. https://doi.org/10.1016/j.jbiomech.2015.10.012.

[16] Synek A. A specimen specific finite element validation study of distal radius fracture osteosynthesis. diploma thesis. Technische Universität Wien; 2015.

[17] Lee ES, Goh TS, Heo JY, Kim YJ, Lee SE, Kim YH, et al. Experimental Evaluation of Screw Pullout Force and Adjacent Bone Damage According to Pedicle Screw Design Parameters in Normal and Osteoporotic Bones. Applied Sciences 2019;9:586. https://doi.org/10.3390/APP9030586.

[18] Moser JE, R Kunkel KA, Acvs D, Gerard PD, John Moser CE. Pullout strength of 2.0mm cancellous and cortical screws in synthetic bone. Veterinary Surg. 2017;46:1110–5. https://doi.org/10.1111/VSU.12692.

[19] Chevalier Y, Matsuura M, Krüger S, Fleege C, Rickert M, Rauschmann M, et al. Micro-CT and micro-FE analysis of pedicle screw fixation under different loading conditions. J Biomech 2018;70:204–11. https://doi.org/10.1016/J.JBIOMECH.2017.12.023.

[20] Ahn SJ, Leesungbok R, Lee SW, Heo YK, Kang KL. Differences in implant stability associated with various methods of preparation of the implant bed: an in vitro study. J Prosthet Dent 2012;107:366–72. https://doi.org/10.1016/S0022-3913(12)60092-4.

[21] Turkyilmaz I, Sennerby L, McGlumphy EA, Tözüm TF. Biomechanical Aspects of Primary Implant Stability: a Human Cadaver Study. Clin Implant Dent Relat Res 2009;11:113–9. https://doi.org/10.1111/J.1708-8208.2008.00097.X.

[22] Pommer B, Hof M, Fädler A, Gahleitner A, Watzek G, Watzak G. Primary implant stability in the atrophic sinus floor of human cadaver maxillae: impact of residual ridge height, bone density, and implant diameter. Clin Oral Implants Res 2014;25:e109–13. https://doi.org/10.1111/CLR.12071.

[23] Liebsch C, Zimmermann J, Graf N, Schilling C, Wilke HJ, Kienle A. In vitro validation of a novel mechanical model for testing the anchorage capacity of pedicle screws using physiological load application. J Mech Behav Biomed Mater 2018;77:578–85. https://doi.org/10.1016/J.JMBBM.2017.10.030.

[24] Schulze M, Gehweiler D, Riesenbeck O, Wähnert D, Raschke MJ, Hartensuer R, et al. Biomechanical characteristics of pedicle screws in osteoporotic vertebrae—Comparing a new cadaver corpectomy model and pure pull-out testing. Journal of Orthopaedic Research 2017;35:167–74. https://doi.org/10.1002/JOR.23237.

[25] Born CT, Karich B, Bauer C, von Oldenburg G, Augat P. Hip screw migration testing: first results for hip screws and helical blades utilizing a new oscillating test method. J Orthopaedic Res 2011;29:760–6. https://doi.org/10.1002/JOR.21236.

[26] Wolfram U, Wilke HJ, Zysset PK. Damage accumulation in vertebral trabecular bone depends on loading mode and direction. J Biomech 2011;44:1164–9. https://doi.org/10.1016/J.JBIOMECH.2011.01.018.
[27] Khorshidparast S, Akhlaghi P, Rouhi G, Barikani H. Measurement of bone damage caused by quasi-static compressive loading-unloading to explore dental implants stability: simultaneous use of in-vitro tests, μ-CT images, and digital volume correlation. J Mech Behav Biomed Mater 2023;138:105566. https://doi.org/10.1016/J.JMBBM.2022.105566.
[28] Ovesy M, Voumard B, Zysset P. A nonlinear homogenized finite element analysis of the primary stability of the bone–implant interface. Biomech Model Mechanobiol 2018;17:1471–80. https://doi.org/10.1007/S10237-018-1038-3/TABLES/4.
[29] Silva-Henao JD, Synek A, Pahr DH, Reisinger AG. Selection of animal bone surrogate samples for orthopaedic screw testing based on human radius CT-derived bone morphology. Med Eng Phys 2022;103:103786. https://doi.org/10.1016/j.medengphy.2022.103786.
[30] Varga P, Grünwald L, Inzana JA, Windolf M. Fatigue failure of plated osteoporotic proximal humerus fractures is predicted by the strain around the proximal screws. J Mech Behav Biomed Mater 2017;75:68–74. https://doi.org/10.1016/J.JMBBM.2017.07.004.
[31] Ovesy M, Indermaur M, Zysset PK. Prediction of insertion torque and stiffness of a dental implant in bovine trabecular bone using explicit micro-finite element analysis. J Mech Behav Biomed Mater 2019;98:301–10. https://doi.org/10.1016/J.JMBBM.2019.06.024.
[32] Steiner JA, Christen P, Affentranger R, Ferguson SJ, van Lenthe GH. A novel in silico method to quantify primary stability of screws in trabecular bone. J Orthopaedic Res 2017;35:2415–24. https://doi.org/10.1002/JOR.23551.